Subwavelength Optical Imaging through a Metallic Nanorod Array

Atsushi Ono,[1,2] Jun-ichi Kato,[2] and Satoshi Kawata[1,2,*]

[1]*Department of Applied Physics, Osaka University, Suita, Osaka 565-0871, Japan*
[2]*Nanophotonics Laboratory, RIKEN, Wako, Saitama 351-0198, Japan*

(Received 19 July 2005; published 28 December 2005)

We propose a subwavelength imaging system without a lens or a mirror but with an array of metallic nanorods. The near-field components of dipole sources were plasmonically transferred through the rod array to reproduce the source distribution in the other side. We calculated the field distribution at the different planes of imaging process using the finite-difference time-domain algorithm and found that the spatial resolution was 40 nm given by the rod size and spacing. A typical configuration is a hexagonal arrangement of silver rods of 50 nm height and 20 nm diameter. We also show that the image formation highly depends on the coherence and the polarization of the source distribution and the source-array distance.

DOI: 10.1103/PhysRevLett.95.267407 PACS numbers: 78.20.Bh, 78.66.Bz, 42.25.Bs, 42.82.Et

A metallic nanostructure with a distinct shape and arrangement exhibits interesting optical properties and has potential for a variety of applications in imaging, lithography, optoelectronic devices, and biosensors [1,2]. It is well known that gold nanoparticles in glass exhibit a reddish color and their mechanism and spectral response were thoroughly studied by Maxwell-Garnett in 1904 [3]. In 1994, Kawata and Inouye proposed the use of a sharpened metallic tip as a probe in near-field scanning optical microscopy [4]. This configuration has been applied to nanoimaging and analysis, including infrared absorption [5], spontaneous Raman scattering [6], and coherent anti-Stokes Raman scattering [7]. Nie and Emory reported the detection of Raman scattering signal from a single molecule adsorbed on a metal particle or aggregated with an enhancement factor of 10^{14-15} [8]. Halas and her group showed that a concentric metallic nanoshell strongly couples with resonant surface plasmons at the near-infrared spectra and applied this technology to biological sensors and labels [9]. Ebbesen's group discovered that periodically arranged nanoslits or nanoholes in metal film beam anomalous light as a collection of surface plasmon polaritons (SPPs) [10–12]. In this Letter, we report subwavelength image transfer, which is another interesting property of metallic nanostructures. The structure we propose is a metallic nanorod array. The function of this structure is similar to that of Pendry's superlens silver film [13,14], but the mechanism is different as discussed later.

Figure 1(a) shows the configuration of a silver nanorod array structure. The typical array arrangement is hexagonal. We define diameter d, height h, and pitch a as the structural values of the array. The rod diameter and the pitch are much shorter than the wavelength, while the height can be longer than the wavelength. We numerically investigated the mechanism of plasmonic image transfer with the finite-difference time-domain (FDTD) calculation in three dimensions. In the calculation, structural values d, h, and a are set to 20, 50, and 40 nm, respectively. The rod axis is parallel to z axis. The calculation volume is $200 \times 200 \times 130$ nm^3 for x, y, and z directions, and the unit cell size is $1 \times 1 \times 1$ nm^3. We iterate 5400 steps of the field calculations to achieve convergence. The permittivity of silver is set as $\varepsilon = -9.121 + i0.304$ at 488 nm [15].

In the simulation, we use point sources shaped as the letter "λ" as an object [Fig. 1(b)]. The point sources are all z polarized but incoherently oscillating as fluorescent

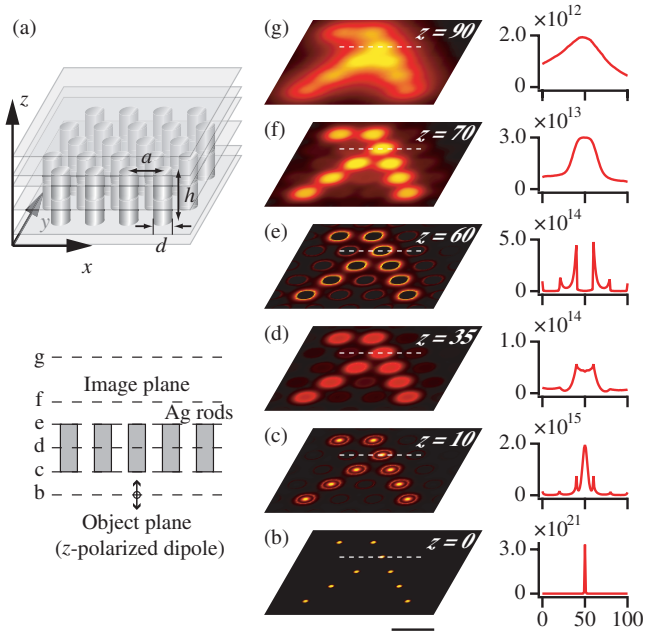

FIG. 1 (color). Subwavelength plasmonic image transfer of a character pattern "λ" with a metallic nanorod array device. (a) The structural model of the device, which is constructed by hexagonally arranged silver nanorods of 20 nm diameter, 50 nm height, and with 40 nm pitch, respectively. (b)–(g) Field propagation process in the image transfer obtained at each longitudinal position by the FDTD simulation. The character pattern is composed of an array of z-polarized dipoles. Left side images show the cross-sectional intensity distributions in the x-y plane. The plots on the right side show the cross-sectional line profiles of dashed lines in the left images. The object plane and imaging plane are defined as $z = 0$ and $z = 70$ nm. The operation wavelength is 488 nm. The size of the scale bar is 50 nm.

 © 2005 The American Physical Society

molecules. Each source is located at the center of a rod. The nanorod array is located 10 nm away from the point sources. Figure 1(c) shows the intensity distribution in the plane at the bottom of the rods, where we see a circular spot and a ring for each point source. The intensity profile crossing the center of a rod (dashed line) is shown in the right half of the figure. Figure 1(d) shows the intensity distribution at $z = 35$ nm, the middle point of the rod. The intensity is attenuated in this plane. In Fig. 1(e), the rings without inner spots appear again at the top of the rod array. Figure 1(f) is the intensity distribution at the plane 10 nm away from the rod array. The FWHM of each spot is 30 nm, and the letter λ is well resolved. Figure 1(g) shows the intensity distribution at $z = 90$ nm, or 30 nm far from the rod array. Spots are blurred and connected with each other, while the letter λ is still clearly resolved. This result shows that the nanopattern is image transferred through a metallic nanorod array, containing the subwavelength resolution. The spatial resolution is 40 nm ($\lambda/12$), which is much beyond the diffraction limit, but is limited by the pitch a of rod array.

To find out the contribution of SPPs we plot polarization components of the field. Figures 2(a) and 2(b) show the distributions of z- and x-polarization components, E_z and E_x, in the vertical cut including a rod center. In Fig. 2(a), it is seen that the E_z component is enhanced at the circumference of the top end of the rod. In Fig. 2(b), the E_x field is enhanced at the side of the rod.

The results in Figs. 2(a) and 2(b) give us the mechanism of the image transfer shown in Fig. 1. A z-polarized dipole source near the entrance surface of a nanorod excites a longitudinal electron oscillation along the rod. This oscillation corresponds to the fundamental mode of the SPP resonance. The oscillating $|E_z|^2$ field is enhanced at the rod end to provide the intensity of subwavelength image. The spot diameter is as small as that of the rod. It is well known that this resonant frequency depends on the aspect ratio of the rod height to the diameter [16,17]. To obtain Fig. 2, we purposely chose the structural values, rod height h and diameter d, to have a resonance of plasmon oscillation for Ar^+ laser excitation at the wavelength 488 nm.

Compared with Pendry's superlens [13,14], which is based on the excitation of the lateral propagation mode of SPP on the entrance surface of metallic film to generate subwavelength field distribution in the exit surface, in our rod array system the longitudinal resonance mode of plasmon on the individual rod is excited to produce a hot spot in the end of rod. The excitation frequency in our case should be at the resonant frequency of SPP mode of rod determined by the aspect ratio. On the contrary, the excitation frequency in Pendry's metallic film should be at the impedance matching frequency of the film surface.

Figure 2(c) shows the total intensity distribution. The right-hand side of the figure shows the intensity profile along rod axis a-a', and the graph at the bottom shows the

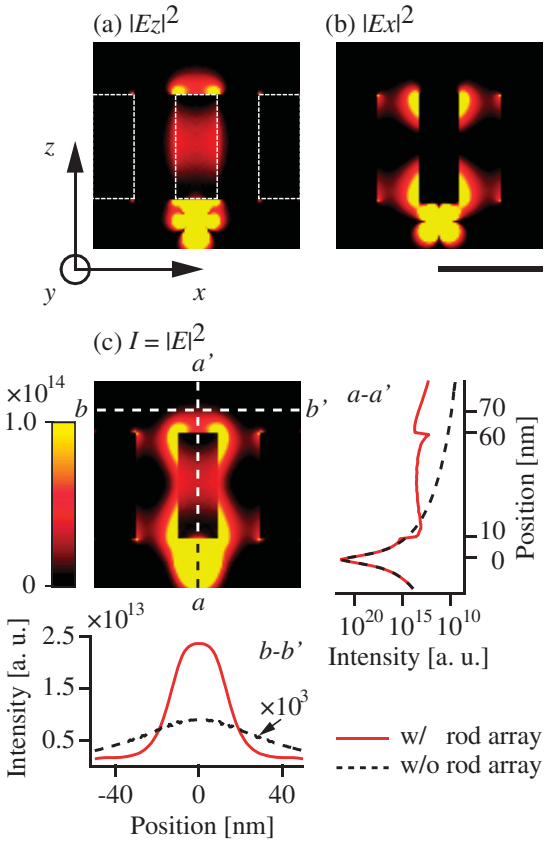

FIG. 2 (color). Intensity distributions for individual polarization components obtained at the vertical (x-z) cross section of the nanorod array including the centric rod axis and a dipole source; (a) $|E_z|^2$ for z polarization, (b) $|E_x|^2$ for x polarization, and (c) $|E|^2$ for the intensity, respectively. Line profiles of the intensity on the rod center (a-a') and on the image plane (b-b') are plotted at the right (log plot) and under sides (linear plot) of the $|E|^2$ distribution. Solid lines correspond to the intensity profiles with a nanorod array, and dashed lines correspond to that without a nanorod array. The size of the scale bar is 50 nm.

intensity profile along the line b-b' at $z = 70$ nm (10 nm apart from the rod exit). In each graph, a dashed line shows the intensity profile when a rod is absent, and a solid line shows the case when the rod exists. When a rod is absent, the intensity decays in propagation, whereas when the metallic rod is present, intensity is preserved due to the plasmon resonance or it even increases at the exit of the rod. In the lateral line profile, the peak intensity with the metallic rod is 2.8×10^3 times higher than that without the rod. Notice that the dashed line in lateral cut for the rod-absence case is 10^3 times magnified in the graph, and the intensity for the vertical cut is in the log scale.

Intensity decreases from rod bottom at $z = 10$ nm to rod top at $z = 60$ nm by 40% [see the right part of Figs. 2(c), 1(c), and 1(e)]. The intensity decreases exponentially due to the absorption loss in metal if the length is infinite, while it may increase by plasmon resonance when the length is

finite. In the case of our simulation, the fundamental mode of plasmon resonance is excited at the given frequency ($\lambda = 488$ nm). The higher order modes for longer rods can be also excited at the same frequency. The propagation length of SPP along a nanorod was theoretically investigated [18] and an experimental result of SPP propagation along a nanowire was also reported [19,20].

Figure 3(a) shows peak intensity (dots) and diameter (FWHM) (triangles) of spot in the image plane as a function of source-array distance. Peak intensity decays as distance increases and it fits well to an exponential decay curve (dashed curve in the figure). This indicates that a major contribution to plasmon coupling with the dipole radiation is the evanescent components of near-field photons. Since the photon transfer is dominantly taken with near-field photons, super-resolution exceeding the diffraction limit is made similar to that of near-field scanning optical microscopy. Indeed, the width of the spot is not blurred but is independent to the source-array distance, as seen in Fig. 3(a).

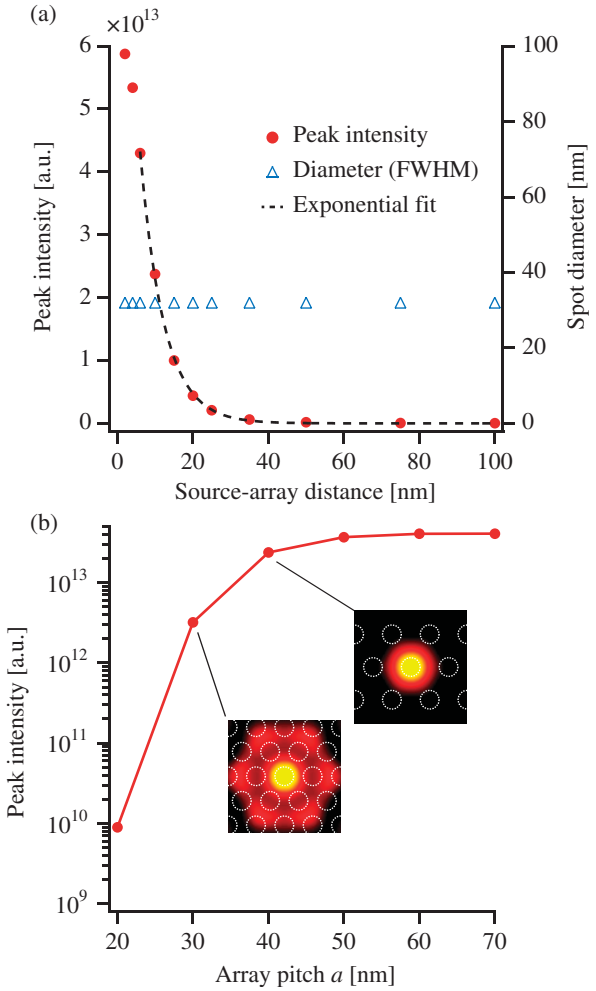

FIG. 3 (color). (a) Relationship between the peak intensity (dots) and the FWHM spot diameter (triangles) as the function of the source-array distance and exponential fitting for the dot marks (dashed curve); (b) hexagonal pitch dependence of the peak intensity at the image plane. Insets show the intensity distributions of the image obtained with the array pitch of 30 and 40 nm. Although the peak intensity decreases in proportional to the source-array distance, the nanorod array always images with a subwavelength resolution. The peak intensity becomes smaller as the pitch decreases. The image becomes broadened at a less than 40 nm pitch because of SPP coupling with surrounding rods.

Figure 3(b) shows the peak intensity at the image plane as a function of array pitch a. The peak intensity becomes smaller as the array pitch decreases. When the distance between rods is less than 40 nm, there is the coupling between SPPs in the neighboring rods, and then coupling out or smearing of the peak intensity occurs. When the rod pitch is larger than 40 nm, SPP coupling between rods becomes negligible. We chose a pitch of 40 nm in our model, since the image resolution depended on the pitch.

We are also interested in the coherence of the dipole sources. Figure 4(a) shows the image of hexagonally aligned six dipoles in a coherent oscillation of *in phase*. The SPPs resonating on six rods surrounding a central rod constructively couple to SPPs on the centric rod to generate

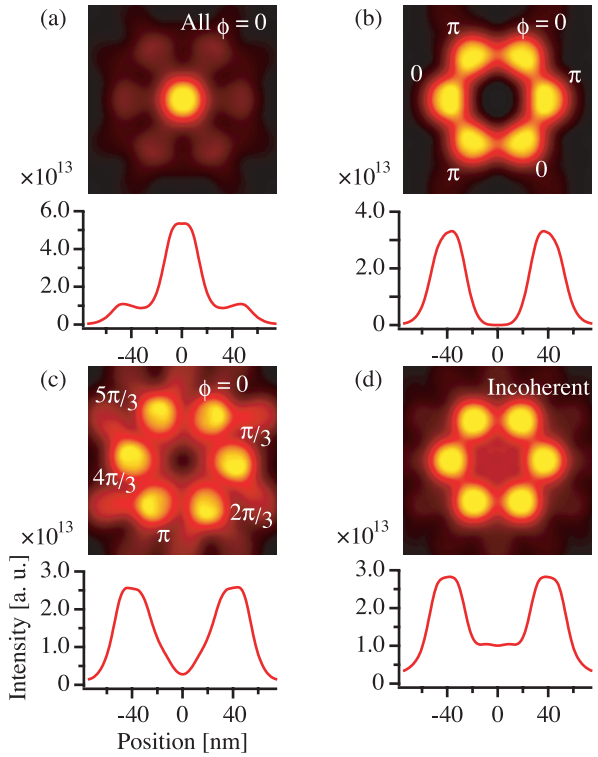

FIG. 4 (color). Images of hexagonally aligned six dots in different dipole oscillation conditions. Each of the six dipoles is placed beneath each rod encircling a centric rod and they are oscillated with (a) in phase, (b) antiphase, (c) phase delayed $\pi/3$ radian steps in clockwise and (d) incoherent state, respectively. Line profiles show the horizontal cross sections of the output fields. An artifact observed in (a) is generated by the constructive interference effect of the SPP coupling between adjoining rods.

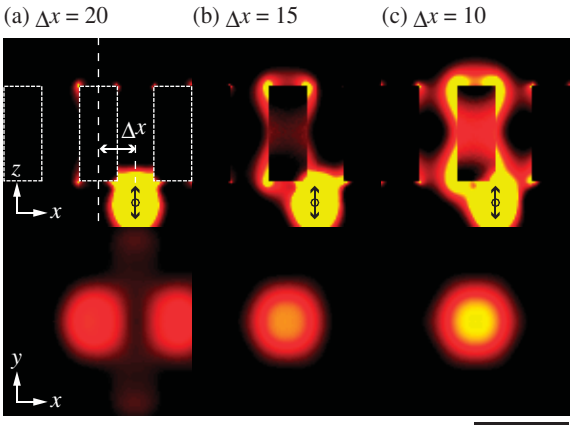

FIG. 5 (color). Field distributions for the location of the point source relative to the rod. Each point source shifts from the rod center to (a) a half of the pitch which is corresponding to the exactly middle point of two rods ($\Delta x = 20$ nm), (b) three-quarters of a half of the pitch ($\Delta x = 15$ nm), and (c) a quarter of the pitch which is at the edge of a rod ($\Delta x = 10$ nm), respectively. Upper figures show the intensity distributions of the vertical (x-z) cross section of the nanorod array including the centric rod axis and a dipole source. Lower figures show the intensity distributions at the image plane above the nanorod array. The plasmon at the most neighboring rod is excited for the dipole source except for the middle point condition. The size of the scale bar is 50 nm.

a bright spot on the center rod. Figure 4(b) shows the intensity distribution when the oscillations of sources are in *antiphase* by next. In this condition, the destructive interference of SPPs at surrounding rods does not produce an artificial spot at the center. In Fig. 4(c), phase of oscillation is every $\pi/3$ radian step different. There is no spot at the center but six spots in outer six rods. Figure 4(d) is the same as others except that the sources are incoherent with each other, so that we do not see any interferometric effect. We conclude that source coherence provides difference in imaging performance similar to that of the conventional optical imaging system, except that the resolution through a rod array is much beyond the diffraction limit. For a coherent source system, the filling ratio of rods should be reduced, for example, by increasing the pitch separation between the rods to suppress the interaction between them.

Up to here, dipole sources are assumed to locate below the rod center. If the source is exactly located at the middle point of rods, the field is equally distributed to two or three rods [Fig. 5(a)]. When the source slightly shifts from this critical condition, in between two or three rods, the plasmon at the nearest single rod is the most excited as shown in Figs. 5(b) and 5(c). Therefore, the resultant image resolution is still determined by the rod pitch.

In conclusion, the metallic nanorod array is numerically confirmed to be a useful device for super-resolution near-field imaging. The resolution in the case of our used parameters was 6 times higher than that of conventional diffraction-limited optics. Our device enables a deep transfer of image without loss and has the ability of parallel image transfer. To realize this super-resolution in image transfer systems, we devise the fabrication method. The rods will be buried in dielectric materials such as glass, polymer, or alumina. Accordingly, the structural parameters are to be optimized as a function of optical frequency.

This work is supported by CREST, Japan Corporation of Science and Technology (JST).

*Electronic address: kawata@riken.jp

[1] *Optical Properties of Nanostructured Random Media*, edited by V. M. Shalaev (Springer, Berlin, 2002).
[2] *Near-Field and Surface Plasmon Polaritons*, edited by S. Kawata (Springer, Berlin, 2001).
[3] J. C. Maxwell-Garnett, Philos. Trans. R. Soc. Lond. **203**, 385 (1904).
[4] Y. Inouye and S. Kawata, Opt. Lett. **19**, 159 (1994).
[5] B. Knoll and F. Keilmann, Nature (London) **399**, 134 (1999).
[6] N. Hayazawa, Y. Inouye, Z. Sekkat, and S. Kawata, Chem. Phys. Lett. **335**, 369 (2001).
[7] T. Ichimura, N. Hayazawa, M. Hashimoto, Y. Inouye, and S. Kawata, Phys. Rev. Lett. **92**, 220801 (2004).
[8] S. Nie and S. R. Emory, Science **275**, 1102 (1997).
[9] E. Prodan, C. Radloff, N. J. Halas, and P. Nordlander, Science **302**, 419 (2003).
[10] T. W. Ebbesen, H. J. Lezec, H. F. Ghaemi, T. Thio, and P. A. Wolff, Nature (London) **391**, 667 (1998).
[11] H. J. Lezec, A. Degiron, E. Devaux, R. A. Linke, L. Martín-Moreno, F. J. García-Vidal, and T. W. Ebbesen, Science **297**, 820 (2002).
[12] W. L. Barnes, A. Dereux, and T. W. Ebbesen, Nature (London) **424**, 824 (2003).
[13] J. B. Pendry, Phys. Rev. Lett. **85**, 3966 (2000).
[14] N. Fang, H. Lee, C. Sun, and X. Zhang, Science **308**, 534 (2005).
[15] P. B. Johnson and R. W. Christy, Phys. Rev. B **6**, 4370 (1972).
[16] J. R. Krenn, G. Schider, W. Rechberger, B. Lamprecht, A. Leitner, F. R. Aussenegg, and J. C. Weeber, Appl. Phys. Lett. **77**, 3379 (2000).
[17] G. Schider, J. R. Krenn, A. Hohenau, H. Ditlbacher, A. Leitner, F. R. Aussenegg, and W. L. Schaich, Phys. Rev. B **68**, 155427 (2003).
[18] J. Takahara, S. Yamagishi, H. Taki, A. Morimoto, and T. Kobayashi, Opt. Lett. **22**, 475 (1997).
[19] R. M. Dickson and L. A. Lyon, J. Phys. Chem. B **104**, 6095 (2000).
[20] J. C. Weeber, A. Dereux, C. Girard, J. R. Krenn, and J. P. Goudonnet, Phys. Rev. B **60**, 9061 (1999).